



# Influence of welding stresses on relief cracking during heat treatment of a creep-resistant 13CrMoV steel Part III: assessment of residual stresses from small-scale to real component welds

D. Schroepfer<sup>1</sup> · A. Kromm<sup>1</sup> · T. Lausch<sup>1</sup> · M. Rhode<sup>1,2</sup> · R. C. Wimpory<sup>3</sup> · T. Kannengiesser<sup>1,2</sup>

Received: 15 December 2020 / Accepted: 24 February 2021 / Published online: 24 March 2021  
© The Author(s) 2021

## Abstract

For higher operational temperatures and pressures required in petrochemical plants, the modified 13CrMoV9-10 steel was developed providing high resistance against creep and compressed hydrogen. Extreme care during the welding procedure is necessary for this steel, attributed to low toughness, high strength in as-welded state, and increased susceptibility to stress relief cracking (SRC) during post-weld heat treatment (PWHT). Previous research of SRC in creep-resistant steels discussed mainly thermal and metallurgical factors. Few previous findings addressed the influences of welding procedure on crack formation during PWHT considering real-life manufacturing conditions. These investigations focus on effects of welding heat control on stresses during welding and subsequent PWHT operations close to realistic restraint and heat dissipation conditions using a special 3D testing facility, which was presented in parts I and II of this contribution. Part III addresses investigations on residual stress evolution affecting crack formation and discusses the transferability of results from large-scale testing to laboratory-scale. Experiments with test set-ups at different scales under diverse rigidity conditions and an assessment of the residual stresses of the weld-specimens using X-ray (surface near) and neutron diffraction analysis (bulk) were performed. This study aims to provide a way of investigating the SRC behaviour considering component-specific residual stresses via small-scale testing concepts instead of expensive weld mock-ups.

**Keywords** Welding · Creep-resistant steel · Residual stresses · Post-weld heat treatment · Stress relief cracking

## 1 Introduction

Efficiency and flexibility are currently a major concern in the design of modern power plants and chemical processing facilities. The high requirements for economic profitability and in particular climate change neutrality are driving this development. Consequently, plant equipment and chemical reactor

components are designed for higher operating pressure and temperature. Creep-resistant low alloyed CrMo steels have been used as constructional materials for decades but have operational limitations, for example the resistance against high-temperature hydrogen attack in petrochemical reactors [1]. For that purpose, 20 years ago, V-modified CrMo steels were developed for use in heavy components like hydrocrackers in the petrochemical industry due to their very good creep-strength and hydrogen pressure resistance at elevated temperatures enabling long service life of the respective components [2]. For example, the 13CrMoV9-10 steel is applicable for process temperatures of up to 482 °C and hydrogen pressures of up to 34.5 MPa [1].

Due to the large dimensions and wall thickness of the reactors (wall thickness up to 475 mm) and the special alloy concept, reliable weld manufacturing of the components is extremely challenging [1]. First, low toughness and high strength of the weld joint in the as-welded condition are critical regarding weld cracking. High welding residual stresses are the result

---

Recommended for publication by Commission II - Arc Welding and Filler Metals

---

✉ D. Schroepfer  
dirk.schroepfer@bam.de

<sup>1</sup> Bundesanstalt für Materialforschung und -prüfung (BAM), Berlin, Germany

<sup>2</sup> Institute for Materials Science and Joining Technology, Otto-von-Guericke-University, Magdeburg, Germany

<sup>3</sup> Helmholtz Centre Berlin for Materials and Energy (HZB), Berlin, Germany

of the highly restrained shrinkage of the component welds. For this purpose, the entire component must be subjected to post-weld heat treatment (PWHT) after completion of the welding operation [2]. The aim is to increase the toughness of the weld joints as well as to reduce the welding induced residual stresses. Before and during PWHT, extreme caution is required to prevent cracking. Unfortunately, V-modified CrMo steels possess an increased susceptibility to cracking during stress relaxation, so-called stress relief cracking (SRC) [3].

Available literature studies have largely focused on thermal and metallurgical factors [3]. However, little attention has been paid on the influence of the welding procedure on crack formation during PWHT considering actual manufacturing conditions (Fig. 1) [4, 5]. For that reason, these investigations focussed on the influence of welding heat control on the mechanical properties by simulating actual manufacturing conditions prevailing during the construction of petrochemical reactors using a special testing facility with a maximum load spectrum of 2 MN for tension or compression (2-MN-testing facility). Focus of part I was the influence of the welding heat control on mechanical stresses and the effect on cracking during PWHT [6]. Part II was mainly dedicated to the metallurgical causes of SRC during PWHT and the interaction with the occurring mechanical stresses [7]. It was shown that high welding-induced stresses due to an increased weld heat input cause a higher susceptibility for SRC formation, see Fig. 2. A further intensification of SRC was observed by an altered precipitation behaviour in the presence of mechanical stresses that are caused by the component-related restraint [7]. The present part III shows how residual stresses, which are present in such welded components and significantly influence the crack formation, can be simulated at the laboratory-scale. As a result, the effect on the residual stresses can be evaluated on simplified small-scale specimens instead of expensive mock-ups, giving the possibility to establish small-scale testing concepts for investigations on SRC behaviour. For this purpose, experiments with test set-ups at different scales and under different rigidity conditions were designed and carried out, cf. Fig. 3 [8]. This study should give an overview of the test set-ups, the

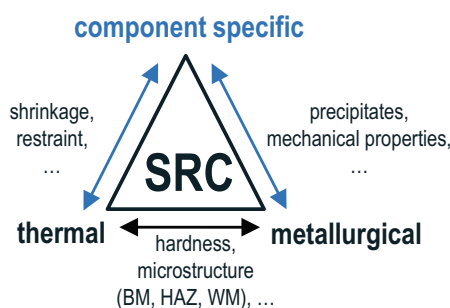


Fig. 1 Influencing factors on SRC [4]

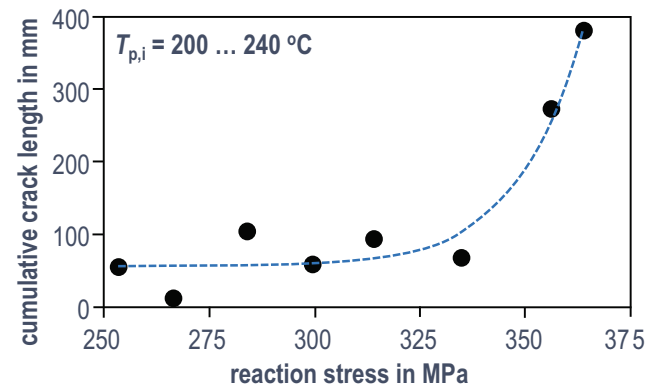


Fig. 2 Cumulative crack length depending on reaction stress before PWHT at weld tests in the 2-MN-testing facility [4, 6, 7]

respective restraint conditions, and the residual stress level and distributions in the welded specimens.

Based on different mock-ups for welding tests [8] and by use of a large-scale testing facility [9], realistic restraint and stiffness situations during welding are to be transferred to small-scale laboratory test specimens for the so-called MVT (Modified Vrestraint Transvarestraint)-test [10, 11] (cf. ISO 17461-3). Starting from the U-shaped notch specimen, a correspondingly high degree of restraint is achieved in the longitudinal direction of the weld seam. Due to the shape of the specimen, a very high weld thicknesses and corresponding realistic supporting effects caused by the complex layer build-up using SAW are provided. However, no significant shrinkage restraints or bending restraints transverse to the weld seam direction can be realised with this sample design. The so-called slot specimens as a mock-up variant of the standardised TEKKEN tests [12], in turn, allow high transverse shrinkage restraints [13, 14]. Sun et al. also used so-called H-form specimens to allow welding under defined constraints transverse to welding direction by experiments and numerical analysis [15]. Due to the lack of transverse stiffeners, the degree of bending restraint for this type of specimen (slot or H-form) is low compared to typical component welds. As the plate thickness or weld seam thickness for SAW welds and, above all, the weld length are rather low, shrinkage restraint in the longitudinal direction is decreased in comparison to the U-shape notch specimen. Instrumentation, handling, and on-line monitoring of forces and deformations during welding are only possible to a limited extent for both mock-up welds. The measurement of strains and stresses along the weld seam in the case of the U-shape notch specimen is impossible without any further effort. For this purpose, the restraint conditions can be transferred to large-scale testing systems, such as the 2-MN-testing facility. It is indeed a fact that even in such tests the weld seam thickness is limited to 25 mm and thus there is no realistic longitudinal shrinkage restraint, as is the case with the U-shape notch specimen. On the other hand, the 3D design of the testing system allows high rigidity

conditions transverse to the welding direction and also high degrees of bending restraint to be achieved. The testing facility is highly instrumentable so that forces and stresses during and after welding as well as during post-weld heat treatment due to the shrinkage restraint of the testing system can be recorded, as already discussed in part I [6]. After the experiments, the residual stresses can be analysed by mobile XRD directly in the facility in the welding vicinity [16]. Welding tests can be reproduced very accurately with this test set-up. However, due to the sample sizes and complexity of the test set-up, the effort to conduct welding experiments is rather high, and the handling is rather difficult. In order to meet these challenges and to offer a straightforward test set-up with which realistic component-related, but also thermal and metallurgical influences on SRC formation can be tested and investigated in an efficient and convenient manner, e.g. for different base and filler materials, the results of mock-up welds and large-scale testing facilities are to be transferred to simple and easily reproducible laboratory specimen formats.

In addition to the use of specimens with high intrinsic stiffness, it is also possible in principle to apply external loads to small specimens. This approach is used in hot cracking tests. In the MVT-test, for example, a bending is initiated during welding. The possibility of applying external loads to the MVT-test specimens during the welding test allows the simulation of restraint intensity factors in the respective bending direction. Thus, different modes (longitudinal or transverse) for restraint intensities are available in the MVT-test by means of the external loads, cf. Fig. 3. For the calculation and quantification of shrinkage restraint and restraint conditions, the concept of

restraint intensity factor was already established in the 1970s by Satoh et al., cf. Fig. 4a–c [18, 19]. The restraint intensity factor in the transverse direction of the weld  $R_{Fy}$  is the spring stiffness  $C$ , based on the seam length  $L_w$ , that the seam has towards the surrounding structure and can be determined for weld joints as shown in Fig. 4c. Bending restraint intensities  $R_{Mx}$  can be calculated accordingly [20]. This is given as bending stiffness around the longitudinal weld seam axis, related to the length of the weld.

Even more complex is the quantification of the degree of restraint in the longitudinal direction of the weld seam, since this depends not only on the length of the weld but also on its surroundings, the build-up of the weld layers, and thickness [15, 20]. The degree of restraint increases with thicker plates and with longer weld seams. Since there is as yet no established method of determining the intensity of restraint in the longitudinal direction analytically or computationally, it shall therefore be in this study classified into 3 levels: high, moderate, and low. It can be assumed that from a weld seam length of 400 mm upwards, high degrees of longitudinal restraint are present [21, 22]. Furthermore, the shrinkage of each weld bead is restrained by the subjacent material or the weld beads below, so that the adjacent cross-section to the longitudinal weld plays a predominant role. Weld seam lengths in the range of 100–300 mm with a plate thickness below 40 mm can therefore be considered to have a comparatively moderate level of longitudinal restraint. A weld seam length <100 mm and weld thickness <10 mm result in low longitudinal restraint intensities.

During welding, the rigidity of the structural design leads to reaction stresses which are superimposed on the

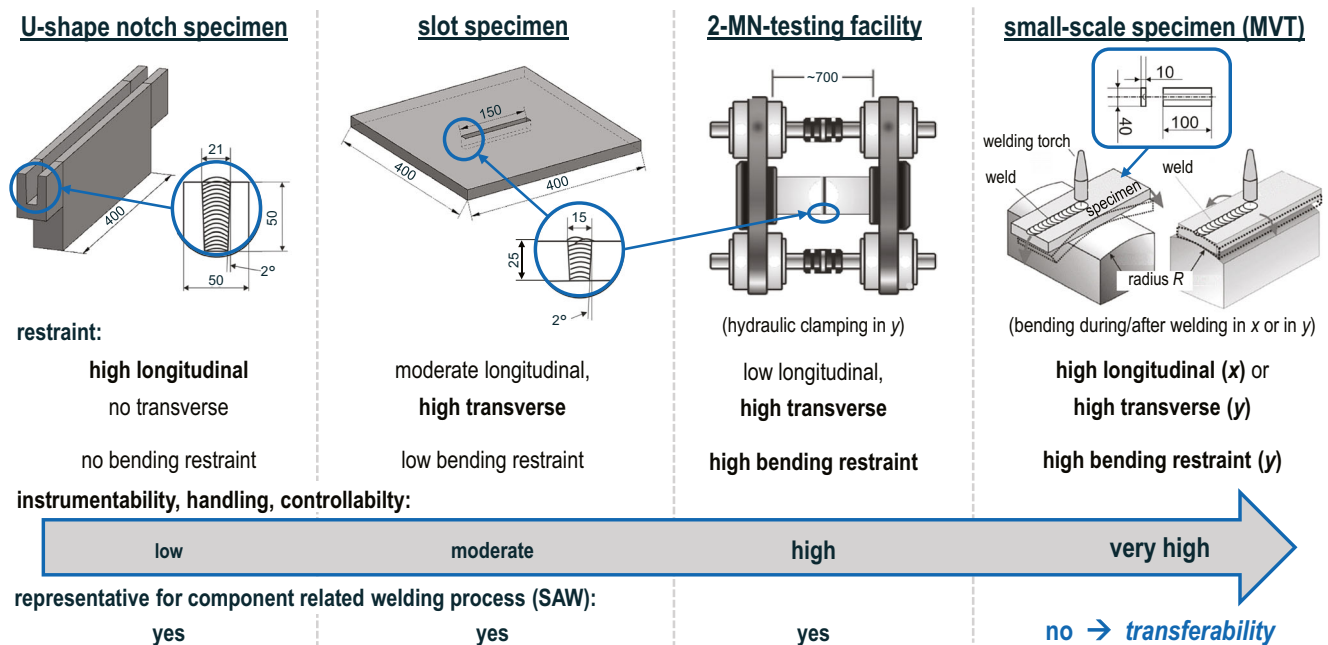
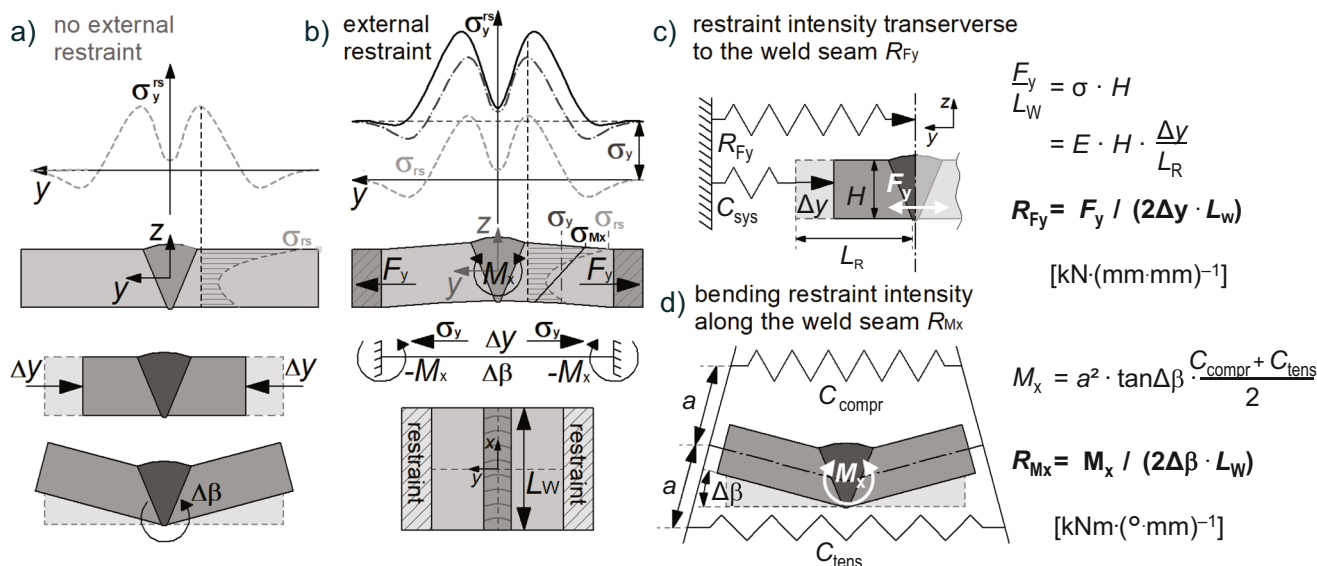


Fig. 3 Different test set-ups at different scales and restraint conditions for SRC testing



**Fig. 4** Schematic for transverse residual stresses: welding under free shrinkage (a) and restraint (b), key parameters for quantification of restraint intensity (c) and bending restraint intensity (d) [13, 17] (with  $\Delta y$ —displacement (weld transverse direction),  $\Delta\beta$ —angular distortion,  $\sigma_{rs}/\sigma_y^{rs}$ —local residual stress,  $\sigma_{Mx}$ —bending stress,  $\sigma_y$ —(normal) reaction

stress,  $F_y$ —reaction forces,  $M_x$ —reaction (bending) moment,  $C_{\text{sys}}/C_{\text{tens}}/C_{\text{compr}}$ —spring stiffness of testing system/compression/tension,  $L_R$ —restrained specimen length,  $H$ —plate/seam thickness,  $a$ —lever arm,  $E$ —Young’s modulus)

local process- and material-related welding residual stresses and thus result in an additional elevation of the residual stresses in the weld seam area and particularly in the HAZ, as can be seen in Fig. 4b. These overall welding stresses are typically considerably relieved in components made of CrMoV steels by PWHT in which the entire component is heated in a furnace. Considering welding tests with small-scale laboratory samples in the MVT-testing facility, these material or component responses can then be simulated with a specific setting or variation of the respective start time, speed, and height, i.e. contact pressure when bending the samples. For this purpose, however, knowledge of the residual stress levels and distributions in real component welds and, in this context, quantitative knowledge of the stiffness conditions present there is a key requirement. Without this knowledge and its systematic investigation, a transfer of the real-life influencing factors to such an investigation of SRC formation in small-scale specimens would not be possible. Inversely, a transfer of the results of small-scale tests for real component welding would also not be appropriate. Based on the results of the experiments and residual stress analysis, our present paper discusses approaches and opportunities to systematically investigate and include all three main influencing factors (cf. Fig. 1), considering their respective complex interactions and interdependencies, in straightforward and easy-to-implement test procedures. The aim is to obtain substantive statements on the SRC behaviour in specific component welds for CrMoV steels and a more in-depth knowledge of the various effects and interactions, particularly regarding component-specific influencing factors.

## 2 Experimental

All submerged arc welding (SAW) experiments were carried out using the low-alloyed creep-resistant steel 13CrMoV9-10 (DIN EN 10028-2). The plates had a thickness of 50 mm and different specimen types were machined, cf. Fig. 3. The chemical composition and the mechanical properties of the base material (BM) and the deposited filler/weld metal (WM) are shown in Table 1. The corresponding welding parameters are shown in Table 2.

All specimens, except the MVT-specimens, were welded using the SAW process (wire diameter 4 mm; slot specimens (cf. Fig. 6b): single DC-mode; 2-MN-test (cf. Fig. 7); and U-shape notch specimens (cf. Fig. 6a): Tandem DC+AC) with multilayer technique, as described in part I. In the MVT-specimens (cf. Figs. 8 and 9), the weld heat input was simulated by GTAW process in an adopted test facility [8]. The heat input for GTAW in the MVT-testing facility is limited due to the welding machine and the specimen dimension or design for this test. According to ISO 17461-3, the recommended highest-level heat input parameters were adopted with  $\sim 1.5$  kJ/mm to ensure the best possible comparability to SAW tests. This MVT-testing facility offers a superimposed mechanical bending of the specimen transverse or longitudinal to the weld direction [10, 11]. Four different conditions have been investigated: (I) bending only, (II) welding only, (III) bending 45 s after welding, and (IV) bending during welding (at half weld length). (I) and (II) were examined as reference conditions. Experiments on (III) and (IV) were realised to simulate load conditions similar to the mock-up and 2-MN-test specimens. In these first transferability tests,

**Table 1** Chemical composition of BM, deposited WM and mechanical properties (at room temperature)

	Content (wt%), Fe balanced									$R_{p0.2}$ (MPa)	$R_m$ (MPa)	$A_5$ (%)
	C	Si	Mn	Cr	Cu	Mo	Ni	V	Nb			
BM	0.12	0.08	0.51	2.29	0.11	0.98	0.12	0.30	0.03	607	725	22
WM	0.07	0.08	1.23	2.27	0.04	0.96	0.16	0.23	0.01	415*	600*	18*

\*Specifications from welding consumable supplier after PWHT at 705 °C for 8 h

all MVT-specimens were analysed in as-welded condition without PWHT, since the initial residual stresses were focussed in this investigation due to their importance regarding SRC. Prior to PWHT, the local residual stresses in the weld seam were analysed in detail and evaluated for each specific case. Residual stress analysis was performed by X-ray diffraction (XRD), cf. Fig. 5a, b, and neutron diffraction, cf. Fig. 5c [23, 24]. The residual stresses at the weld and weld vicinity of each specimen were analysed by XRD using the  $\sin^2\psi$ -technique [24] on the top surfaces across the weld, the HAZ, and the base material using a step size of 1 mm. The neutron diffraction experiments in order to analyse additionally the residual stresses in the bulk, exemplary for the slot specimens, were conducted at the research reactor BER II (instrument E3) at Helmholtz-Zentrum Berlin in Berlin-Wannsee. All principal directions were measured with a gauge volume of  $2 \times 2 \times 2 \text{ mm}^3$ .

Post-weld heat treatment was conducted for 10 h at 705 °C (heating and cooling rate:  $60 \text{ °C h}^{-1}$ ) [6]. The restraint intensities of the specimens were determined by means of computing (FEM), experimental determination, and analytical estimation or calculation [20]. Therefore, the first paragraph of the results part is dedicated to the restraint intensities of the different test-set-ups.

## 3 Results and discussion

### 3.1 Restraint analysis

#### 3.1.1 Self-restraint specimens

The U-shaped notch specimen, as shown in Fig. 6a, is characterised by a high longitudinal rigidity of the weld.

This is due to the length of the specimen. According to commonly established models and concepts, e.g. by the authors of [21, 22], a saturation is reached at a weld seam length of approx. 400 mm, so that from this length a kind of maximum of the restraint level in the longitudinal direction of the seam and thus of the expected welding stresses is achieved. In addition, the groove surrounding the weld, the cross-sectional area below the weld seam, and the stiffness of the specimen in longitudinal direction as well as the section modulus against bending around the  $y$ -axis is very high [15, 20]. Combined with the high weld seam thickness (50 mm) and the complex build-up of the weld seam, this specimen shape leads to a restraint of shrinkage in the longitudinal direction as is to be expected in thick-walled joints of real component welds. The small web width next to the weld seam does not result in any significant hindrance of shrinkage during welding, particularly because the webs are heated up considerably during welding, so that both the restraint intensity transverse to the weld and the intensity of restraint against bending around the weld seam axis are negligible.

The restraint intensity of slot specimens was determined using structural mechanics calculation, cf. Fig. 6b. As already carried out in [13, 16], a distributed load of  $p = 100 \text{ N mm}^{-2}$  was applied to the seam flanks of the model and the mean displacement of the seam flanks was calculated, cf. Fig. 4. These analyses could be simulated and validated by applying a DIC system and the dilatation of the seam opening by means of a hydraulic flange spreader. Thereby the specimen geometry resulted in an approximate  $R_{F_y} = 20 \text{ kN} \cdot (\text{mm} \cdot \text{mm})^{-1}$ . The intensity of bending restraint of the weld seam around the longitudinal direction  $R_{M_x}$  was approximated with analytical methods. For this purpose, the moments of inertia of the remaining webs at the beginning and end of the weld were taken as a basis, relative to the neutral axis of in the centre axis of the

**Table 2** Layer sequence and welding parameters for different test set-ups

Specimen	Number of layers	Load condition	Welding speed (mm/min)	Current (A)	Voltage (V)	Heat input (kJ/mm)
U-shape notch (Fig. 6a)	18	Self-restraint	360	650/500	34/31	~ 6.8
slot specimen (Fig. 6b)	10	Self-restraint	360	600	30	~ 3.0
2-MN-test specimen (Fig. 7)	12–24	External load	420–850	600/550	30/32	2.0–5.0
MVT-specimen (Figs. 8 and 9)	1	External load	120	210	15	~ 1.5

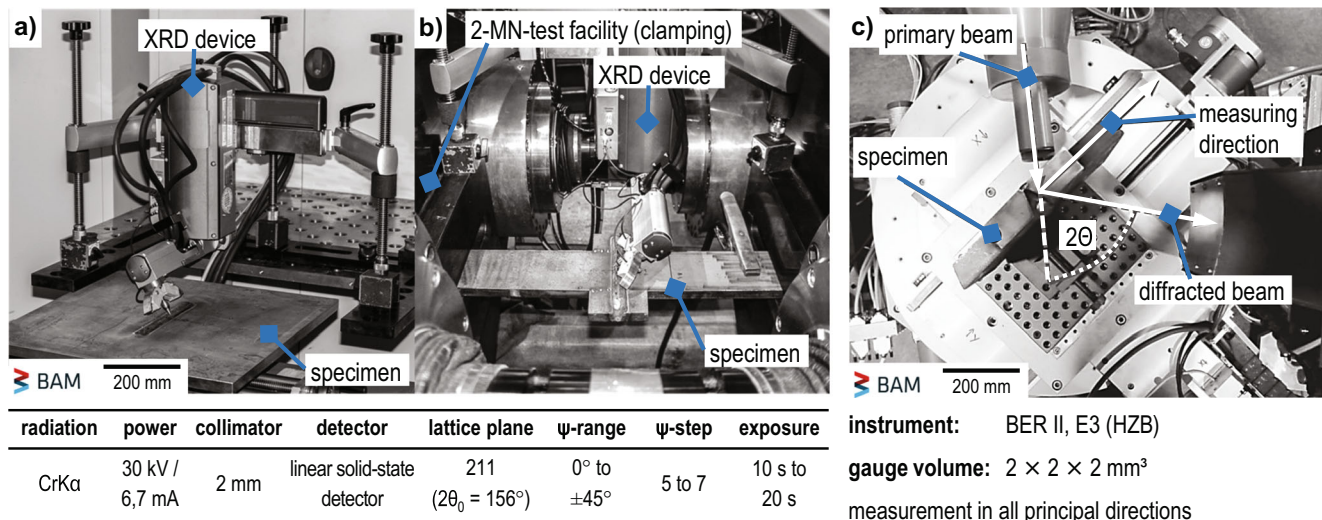


**Fig. 5** Residual stress analysis: X-ray diffraction at mock-up specimens (a) and in the 2-MN-testing facility (b, focus: surface) and neutron diffraction experiments at slot specimens (c, focus: bulk) [23]

weld. Due to the comparatively low specimen thickness (25 mm) and the resulting low lever arms, which inhibit distortion during welding, the intensity of bending restraint is also comparatively low and is approximately just  $R_{Mx} = 0.5 \text{ kNm}(\text{mm})^{-1}$  [13, 16]. The short seam length of the slot specimen of  $L_W = 150 \text{ mm}$ , especially in comparison to the width of the whole specimen, only results in a lower level of restraint in the longitudinal direction of the seam in comparison to rather realistic values in the U-shape notch specimen. On the other hand, due to the slotted specimen shape and the remaining webs at the beginning and end of the weld seam enveloping the weld seam, there is an additional constraint for the longitudinal shrinkage because the flanks of the joining partners are supported by them. This effect was also found by Sun et al., where slots at the beginning/end of the weld seam were prepared to achieve a so-called H-specimen [15]. The longitudinal residual stresses increased significantly with decreasing length of these slots. Consequently, the restraint intensity longitudinal to the weld seam can be characterised as moderate or medium level. Hence, this type of specimen is

particularly suitable for analysing the influence of transverse shrinkage on the welding-related stresses.

### 3.1.2 Restraint due to external load in 2-MN-testing facility

The 2-MN-testing facility has also been specially designed to achieve a preferably high defined shrinkage restraint by means of the rigidity of the hydraulically operated test frame. Due to the knowledge about the rigidity of the system (spring rigidity of the piston rods) and with the given dimensions of the clamped welding sample, the intensity of restraint transverse to the weld direction can easily be determined. With the given dimensions (restraint length  $L_R = 700 \text{ mm}$ , specimen thickness  $H = 25 \text{ mm}$ , weld seam length  $L_W = 250 \text{ mm}$ ) and spring stiffness in the compression direction of the piston rods  $C_{\text{comp}} = 1.222 \text{ kN}(\text{mm})^{-1}$ , the restraint intensity is  $R_{Fy} = 2.7 \text{ kN}(\text{mm} \cdot \text{mm})^{-1}$ , cf. Fig. 7 [9]. This value is below the restraint intensity of the slotted specimens but is certainly representative for structures in these plate thickness ranges. By appropriate measures such as

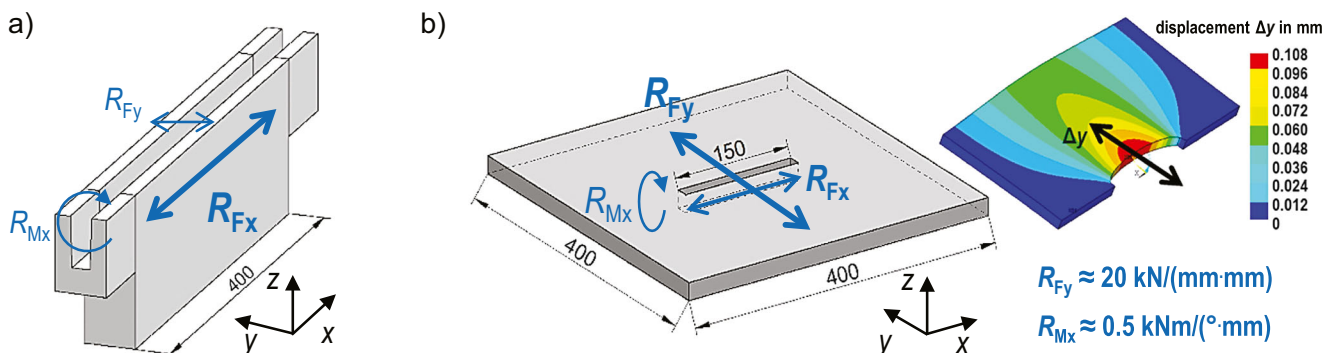


**Fig. 6** Restraint intensities of mock-up test set-ups, U-shape notch specimen (a), slot specimen (b) [13]

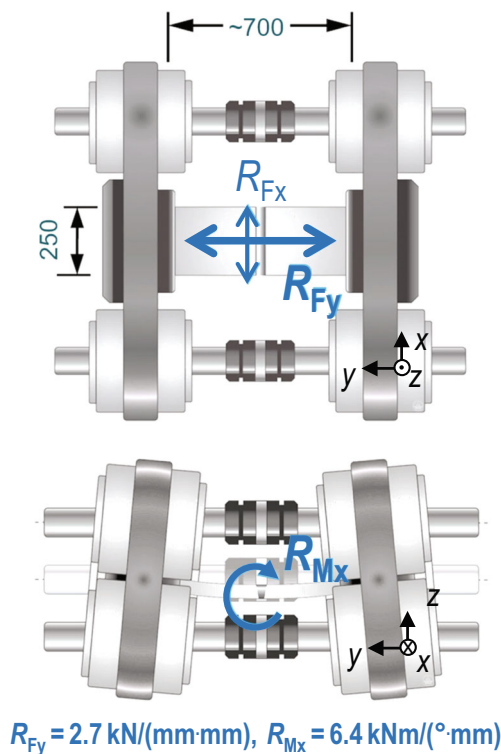


**Fig. 7** Restraint intensities of the experimental set-up in the 2-MN-testing facility [9, 16]

reducing the weld seam length, it is also possible to increase the restraint intensity even further. It should be emphasised that the 3D arrangement of the hydraulic test system in this test system also allows a high restraint of the welding distortion around the  $x$ -axis to be accomplished. This is since two of the piston rods between the test desks are located with a lever arm of  $a = 230 \text{ mm}$  above and below the neutral axis of the weld seam of the specimen. With the relatively high spring stiffness of the piston rods ( $C_{\text{compr}} = 1.222 \text{ kN}\cdot\text{mm}^{-1}$ ;  $C_{\text{tens}} = 1.377 \text{ kN}\cdot\text{mm}^{-1}$ ), a bending restraint intensity of  $R_{Mx} = 6.4 \text{ kNm}/(^{\circ}\cdot\text{mm})^{-1}$  is achieved in terms of a weld seam length of  $L_W = 250 \text{ mm}$ , which is much higher compared to the slotted specimen. Furthermore, the bending moments resulting from this during welding may also be investigated [5, 9, 16].

The restraint intensity in the longitudinal direction is of rather minor importance for this test system, especially with the specimen shape used, as they are only small due to the low weld seam length of  $L_W = 250 \text{ mm}$ , cf. Fig. 7. In contrast to the slot specimen, the weld seam is not enveloped either, so that no webs at the beginning and end of the weld seam contribute to an additional constraint of the longitudinal shrinkage, a phenomenon also been reported by [15]. Thus, a significantly lower restraint intensity in the longitudinal direction of the seam is to be assumed compared to the two mock-up test set-ups. Therefore, the focus of the investigations with this

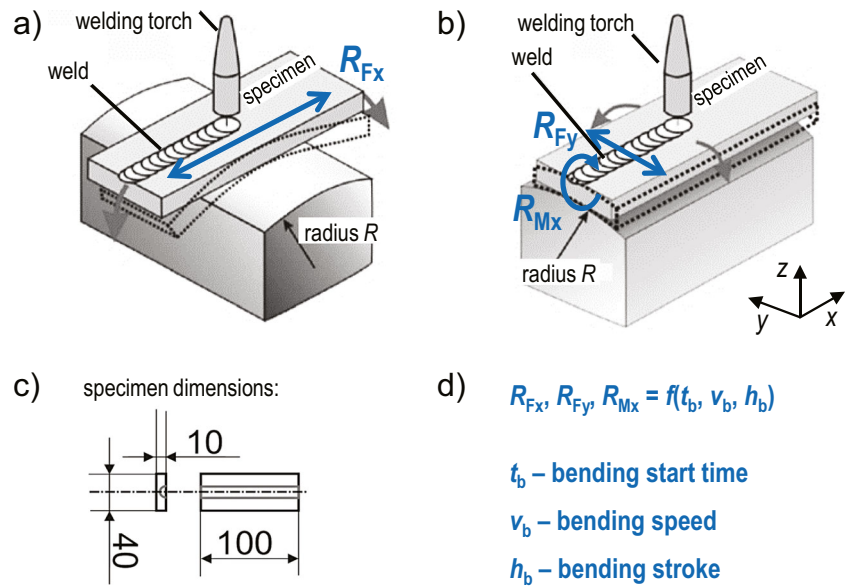
test set-up is on the forces and moments as well as the resulting stresses or bending stresses in the welded specimen transverse to the weld seam.

### 3.1.3 Restraint due to external load for small-scale specimens

Small-scale laboratory specimens do not have significant restraint intensities comparable to mock-up test or large testing facility set-ups. Therefore, an external load has to be superimposed during the weld test in order to simulate restraints or the respective response of the component/material. In this work, an actual hot crack test is supposed to be used to apply stress to small-scale specimens in a welding test. The samples can be exposed to stress in the welding test either in longitudinal or in transverse direction. Thus, only a significant restraint intensity either longitudinally or transversely to the welding direction can be represented with this test set-up, cf. Fig. 8a–c.

The component/material response due to welding depends on the restraint intensity. Hence, this (partially transient) response is to be transferred to the MVT tests in terms of the temporal progression and the level of external load [10]. Therefore, the restraint intensity is a function of the bending start time, bending speed, and bending stroke, cf. Fig. 8d. For a basic analysis of this test method in this study, bending speed (of the hydraulic rams) and (surface) strain were kept constant at  $2 \text{ mm/s}$  or  $4\%$ , respectively. The parameter selection represents the highest bending load achievable with the MVT-testing facility to also provoke most significant effects and considerably high weld seam stresses at moderate bending speed. Note that the bending speed recommended by ISO 17461-3 should not be less than  $1.8 \text{ mm/s}$  and in this initial investigation a parameter selection as similar as possible to the standard testing parameters should be chosen. The bending start time was varied in (I) bending without welding, (II) welding without bending, (III) bending  $45 \text{ s}$  after welding (during cooling), and (IV) bending during welding in longitudinal direction (varestraint mode), cf. Fig. 8a and Fig. 9. These four different settings are basically intended to show the applicability of the test set-up for such investigations and, according to the proposed model, to simulate the following restraint conditions in the longitudinal direction. The first setting, (I) bending only, is a reference test in order to show the solely mechanical influence of the external load on the specimen without the effect of heat input. (II) Welding without bending also has more of a reference character, since a small weld seam without significant shrinkage restraint in the longitudinal direction is represented. This also serves as a reference to the other two tests, where welding and bending are applied. (III) Bending  $45 \text{ s}$  after welding of the weld seam represents the extreme case of a very short weld seam or a very fast welded seam, in which a high restrained shrinkage occurs not until after the seam has been welded. Furthermore, it is assumed that in this case, a significant share of phase transformation during cooling is finished to suppress

**Fig. 8** Restraint due to external load at small-scale specimen in MVT-tests: bending during/after welding in weld direction  $x$  (a) or transverse to weld direction  $y$  (b); specimen dimension (c); influences on the restraint conditions (d) [10]



this effect (transformation stresses) or isolate them from other effects. In the fourth setting, (IV) welding during bending (at half weld length), on the other hand, the opposite extreme case is to be reproduced, i.e. that a very high shrinkage restraint in the case of a very long weld seam or slowly welded seam leads to severe loads already during welding.

## 3.2 Welding stress analysis

### 3.2.1 Self-restraint specimens

In the U-shape notch specimens, the restraint in longitudinal direction is predominant. The low restraint level transverse to the welding direction generates only minor residual transverse stresses over the whole width, see Fig. 10a. As an effect of the longitudinal restraint intensity, high longitudinal residual stresses can be found in the heat affected zone (HAZ) up to 400 MPa, see Fig. 10b. In the weld seam itself, compressive stresses are evident that stem from transformation induced stresses, as described in [25]. Furthermore, the stress level in all directions drops to (0±50) MPa after PWHT at 705 °C.

The slot specimens represent a high degree of transverse restraint in this study. For the investigated specimens, also a significant restraint in longitudinal direction is observed, as a tensile stress level in the HAZ up to 400 MPa is present, see Fig. 11a. Correspondingly, in this case, the quenching and transformation effects on the residual stress evolution according to the current model concepts for steels which are subject to transformation during cooling lead to intensive settlement and to some extent to compressive stresses in the weld metal [26]. The residual stresses in transverse direction, as shown in Fig. 11b, analysed by XRD, are also a result of restraint, quenching, and transformation stresses in the weld metal, leading to a residual stress profile with high stress gradients from compressive to tensile stresses. Note that the initial stress level of the specimen surface is approx. -200 MPa due to the machining of the specimen. It is observable that the stress level in the vicinity of the weld is starting from approx. 200 MPa above the initial stress level and decreases to approx. 50 MPa above the initial stress level. This is in a close agreement with similar experiments in [13].

The residual stresses in the slot specimens were additionally analysed by means of high-energy neutron diffraction to

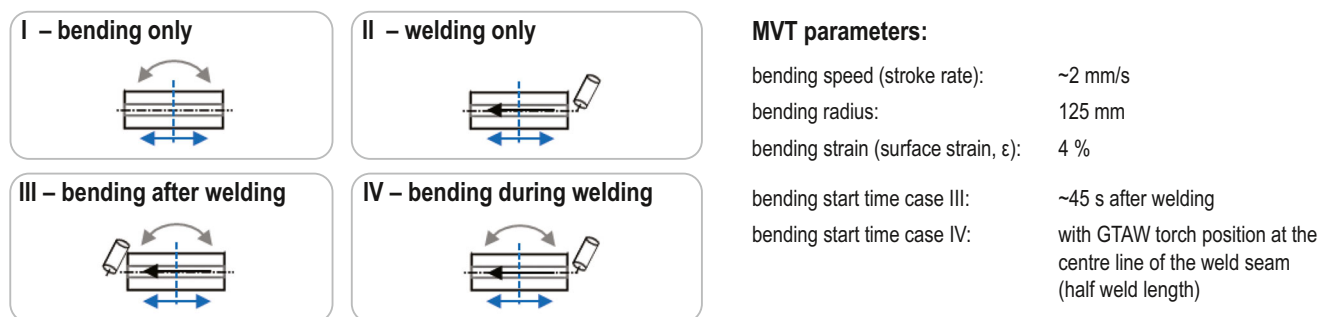


**Fig. 9** Different settings (cases I–IV) of the experiments conducted in the MVT-testing facility and bending parameters



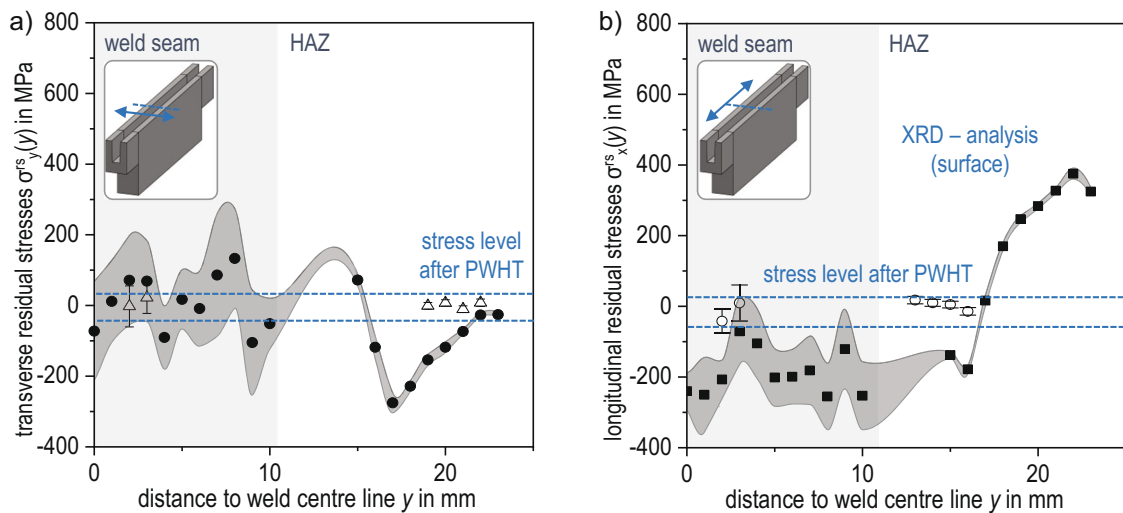


**Fig. 10** Residual stress profiles measured at the U-shape notch specimen using XRD in as welded condition and after PWHT transverse (a) and longitudinal (b) to welding direction

account for the residual stresses in the bulk. Figure 4c shows a transverse residual stress distribution across the weld at the half thickness of the specimen ( $H = 12.5$  mm). High transverse residual stresses at the level of the yield strength of the base material (BM) are obvious in the whole weld seam as a result of the high transversal restraint intensity. Towards the HAZ the residual stresses drop to a stress level of  $(200 \pm 50)$  MPa and with increasing distance to the weld seam, the residual transverse stresses decrease steadily. This corresponds on the one hand to the analysis on the surface by means of XRD and on the other hand to reaction stress measurements for comparable experiments, e.g. described in [8].

After PWHT, the residual stresses are almost completely relaxed. These measurements in the bulk also show that under false assumptions a surface residual stress analyses might be underestimated. The most stringent care must therefore be taken to be able to draw the correct conclusions from the surface analyses by means of residual stress assessment. For

this purpose, it is essential to include effects that can have an impact on the residual stresses on the surface, such as the initial values of the surface residual stresses, quenching effects, phase transformation during cooling in the weld metal or in excessively heated areas, and inhomogeneous and time-shifted transformations and tempering effects during welding and in particular multi-layer welding. For this purpose, the commonly known and established concepts for residual stress evaluation, in particular for transformable steels, shall be applied [20, 25–28].

### 3.2.2 Restraint due to external load in 2-MN-testing facility

A comparable high restraint intensity in transverse direction was achieved by clamping and welding specimens in a special 2-MN-testing facility at BAM Berlin. The residual stress analysis was conducted after welding and cooling prior to PWHT directly on the weld seam of the specimen clamped into the

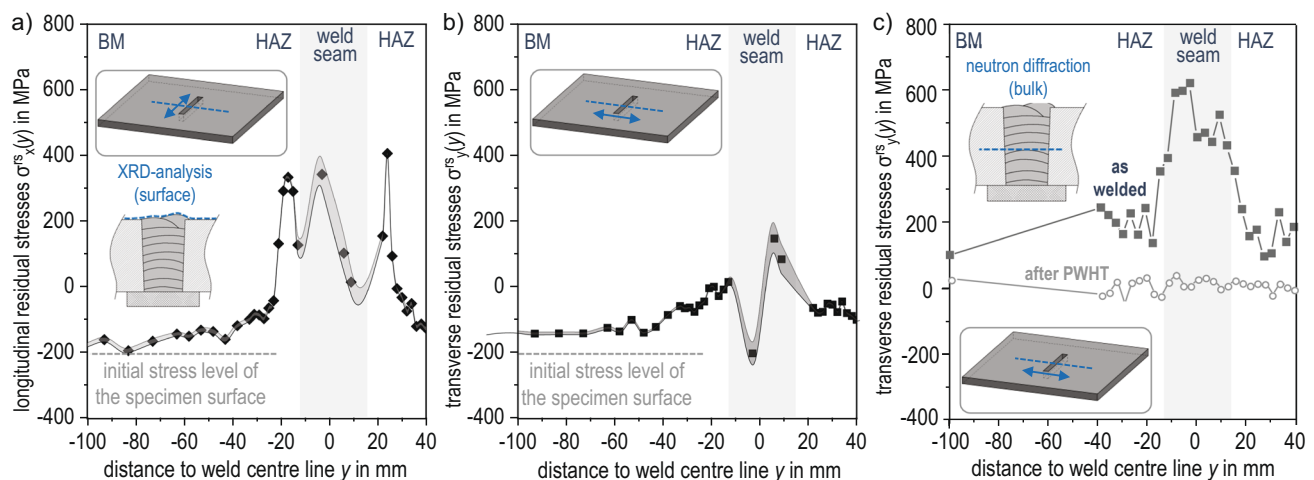


**Fig. 11** Residual stress profiles measured at the slot specimen using XRD in as welded condition longitudinal (a) and transverse (b) to the welding direction and by means of neutron diffraction (c) transverse to the weld direction in as welded condition and after PWHT

testing fixture. Hence, the reaction stresses occurring after cooling are superimposed, as it is the case in the slot specimens. This led to significant transverse residual stresses in the weld seam masked by local effects due to transformation and quenching, see Fig. 4a. As a result, also high stress gradients are the case in this weld seam ranging from tensile stresses (approx. 470 MPa) to compressive stresses (−100 MPa). Starting from the transition zone towards the weld vicinity, the residual stresses decrease to a minimum of approx. −50 MPa. Proceeding from the weld seam in the direction of BM, the residual stresses increase to approx. 300 MPa based on the initial stress level in the BM or HAZ of −200 MPa.

The stress level in the HAZ corresponds with the measured total reaction stresses of approx.  $\sigma_{2MN} = 300$  MPa at to the same heat control parameters regarding the regression model of the test matrix results in part I, cf. Fig. 12b [4]. These results have already been presented and discussed in [16, 29]. They show that the residual transverse stress level in the HAZ corresponds to the total reaction stresses on the top side of the weld (superposition of normal stresses and bending stresses) determined in the welding experiment using the test facility. The reason for these high bending stresses is the high bending restraint intensity of the test set-up in the 2-MN-testing facility and the comparatively high angular distortion during welding with these seam preparation and heat control parameters, which is, therefore, restrained by the fixture. This also shows, in agreement with [13, 16], that the bending restraint has more impact on transverse residual stresses in the HAZ or weld vicinity and less on the residual stresses in the weld metal.

### 3.2.3 Restraint due to external load for small-scale specimens

The residual stresses in the test specimens released from MVT-testing facility after the experiments were analysed by means of XRD in longitudinal direction prior to PWHT. Note that after

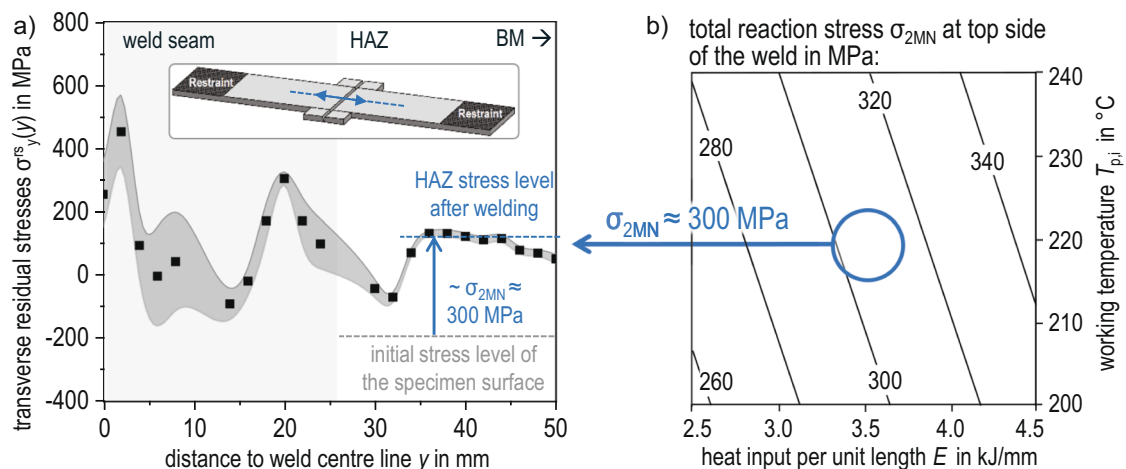


**Fig. 12** (a) Residual stress profile measured using XRD at a welded specimen clamped into the 2-MN-testing facility (including reaction stresses) transverse to the weld; (b) total reaction stresses measured by

PWHT at 705 °C, the residual stresses were reduced to (0±50) MPa. Figure 13 shows an overview of all measured longitudinal residual stresses. The initial residual stresses in the surface of the specimens, which were machined from the BM-plates, are at the magnitude of (−130±30) MPa, cf. Fig. 13a.

**Case I** Sole bending load with a bending strain of  $\varepsilon_{\text{tot}} = 4\%$  and subsequent relief due to the removal of the sample from the MVT-testing facility to perform the residual stress analyses leads to compressive residual stresses of approx. (−275±50) MPa on the surface, resulting from an elastic springback of the sample, cf. Fig. 13a. This behaviour can be attributed to a high tensile stress above the yield point and corresponding plastic deformations on the sample top side during bending, i.e. permanent deformation. The top side is then finally compressed due to the elastic springback accordingly when the sample is relieved by the high elastic component of bending deformation in the lower part of the specimen.

**Case II** Welding only of the specimen affects longitudinal stress distributions as typical for steel with undergoing phase transformation with a comparatively low tensile stresses level of max. 100 MPa at the weld centre, since no restraint or external load was applied, cf. Fig. 13b. Furthermore, the small specimen size and the short weld length do not lead to a considerable restraint while welding and cooling. Near the fusion line compressive stresses down to −200 MPa are obvious, which are due to the volume expansion of the phase transformation while cooling of the weld. Due to the restraint of the cooler weld vicinity, a balancing of these residual compressive stresses is affected as tensile residual stresses with maxima of over 200 MPa in the HAZ.

**Case III** Bending load applied subsequently 45 s after welding reveals the highest tensile residual stresses in the weld seam

means of global forces and stresses after welding and cooling of specimens in the 2-MN-testing facility (prior to PWHT) vs. heat input  $E$  and working temperature  $T_{p,i}$  for the complete test matrix (cf. part I)

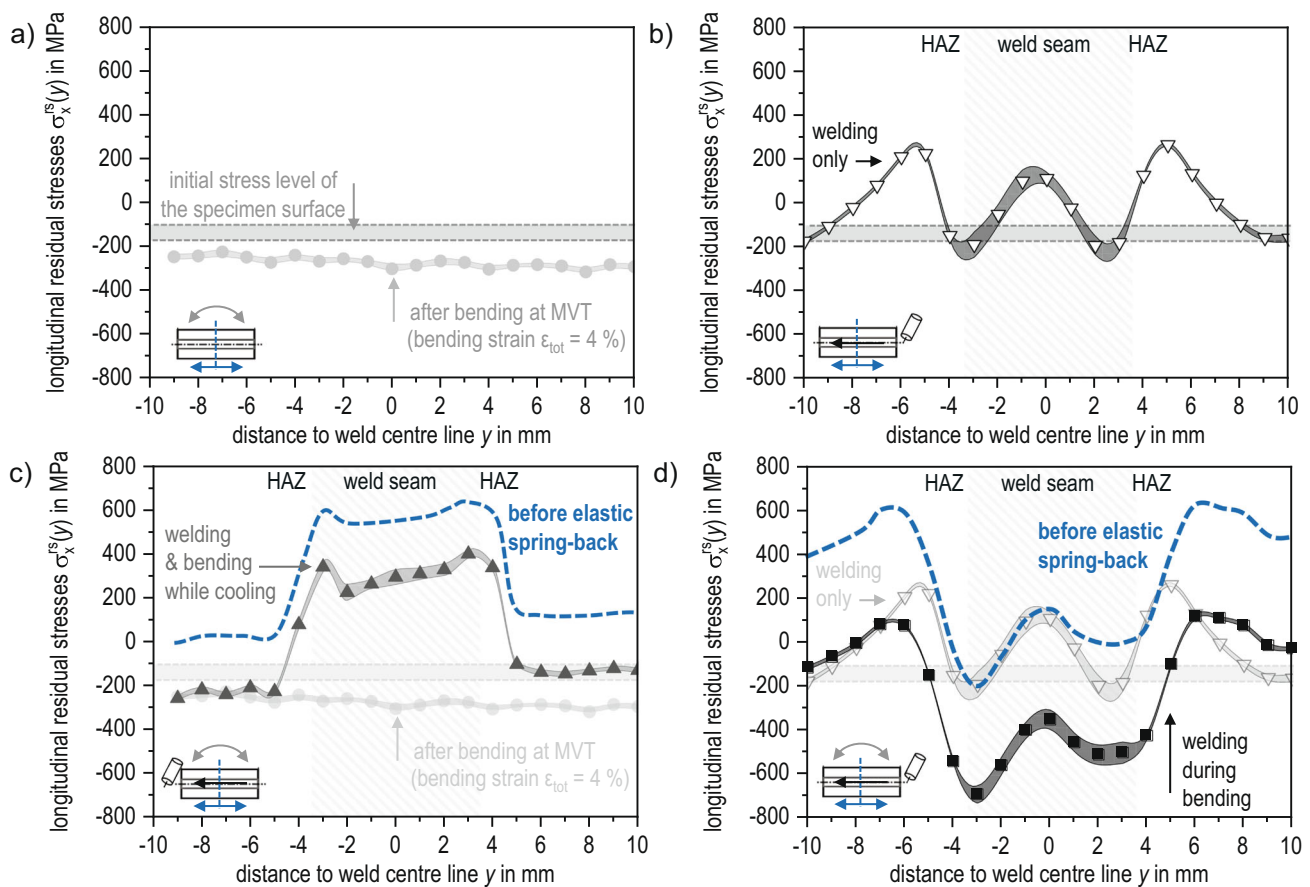


**Fig. 13** Longitudinal residual stress profiles measured after specimen release off the MVT-testing facility using XRD after (I) bending only (a), (II) welding only (b), (III) welding and subsequent bending during cooling (c), and (IV) welding during bending (d)

(approx. 400 MPa), cf. Fig. 13c. The transformation stresses were completely suppressed due to the superimposing bending stresses while cooling. Therefore, no constraints towards the weld vicinity were observed and the residual stresses in the HAZ are at the amount of the initial state. Note that the residual stresses were measured after removal of the specimen from the MVT-testing facility and relief of the bending load. Since the specimen is loaded 45 s after welding, i.e. while cooling of the specimen, and since a considerable part of the specimen is not heated to a high enough temperature, i.e. the heat-resistant steel still allows large amounts of elastic deformation even at high temperatures, a significant amount of elastic springback is to be anticipated. Hence, it can be expected that the residual stresses must have been correspondingly higher before the relief. If it is supposed that, in case I (bending only, cf. Fig. 13a), a relatively uniformly distributed reduction of the stresses takes place over the width of the specimen, it can be concluded that a parallel shift of the residual stress profile corresponding to the amount of springback upwards can be applied in order to be able to draw conclusions about the residual stresses prior to specimen extraction from the MVT-testing facility. In addition, the residual stress distribution in the weld shows a relatively constant plateau of tensile residual stresses

in the weld, which indicates that tensile residual stresses had been reached the yield strength of the material. With both assumptions, a parallel up-shift of the residual stress profile is thus possible, so that the tensile residual stress plateau at the base materials yield strength is attained in the weld area, see Fig. 13c.

**Case IV** Bending load applied during welding, as shown in Fig. 13d, causes a superposition of transient stresses at the weld top side and additional bending stresses at high temperatures while welding. This results in a plastic deformation, since there is almost no resistance against the applied load for the whole weld zone. Hence, after welding, subsequent cooling of the bended specimen causes an evolution of a welding residual stress distribution with higher residual stresses in the weld vicinity due to the higher yield point while welding and bending. In the weld seam, the residual stresses are lower, since bending load is applied when high temperatures and, therefore, a low yield point are present there. In addition, the phase transformation leads to lower residual stresses in the weld and higher stresses in the weld vicinity as shown in case II (welding only, cf. Fig. 13b). It is obvious that the elastic springback from relieving the bending load at room

temperature, i.e. the removal of the specimen from MVT-testing facility, leads to low residual stresses in comparison to case II.

According to the discussion in context with case III (bending after welding, cf. Fig. 13c), a parallel up-shift of the stress, which was released due to the elastic springback, is useful to draw conclusions about the residual stresses after welding and bending, shown in Fig. 13d. Since the transformation stresses and restraint stresses while cooling of the specimen should not be considerably influenced by a bending while welding, a similar residual stress distribution and level is predominant in the weld seam. The bending load and the superimposed constraint of the compressive residual stresses due to phase transformation in the weld seam lead to considerably higher tensile residual stresses in the HAZ and weld vicinity up to 600 MPa (yield point of BM) in comparison to the specimens from cases II to III, cf. Fig. 13b and c.

### 3.3 Result overview and discussion on transferability

In Table 3, an overview of the resulting level of restraints, welding-induced stresses, and location and approx. maximum of the residual stresses is shown. By comparison of the respective stress for each specimen or test set-up, significant effects of the transverse and longitudinal restraints on the resulting welding-induced stresses can be observed.

Welding conditions in which almost no shrinkage is restrained transversely to the weld (U-shape notch specimen, cf. Figs. 6a and 10) naturally show only a very low transverse residual stress level, especially due to the superimposed transformation stresses. Very high transversal restraints as present in the slot specimen (cf. Figs. 6b and 11) lead to considerably increased tensile residual stresses primarily at the weld metal ranging to the level of the yield point of the base metal, especially in the bulk. High transversal restraints in connection with a high restraint of angular distortion (specimen in 2-MN-testing facility, cf. Figs. 7 and 12) cause also high stress level in the weld metal. In addition, these conditions lead to exceedingly high stresses in the HAZ or weld seam vicinity.

The simple implementation of very high shrinkage restraints in the longitudinal direction via the specimen length and weld seam thickness or specimen thickness (U-shape notch specimen, cf. Figs. 6a and 10) leads to very high welding-induced residual stresses in the HAZ and weld seam vicinity, which are due in particular to the support of the compressive transformation residual stresses arising in the weld metal. The slot specimens (cf. Figs. 6b and 11) with lower longitudinal shrinkage restraint compared to the U-shape notch specimens also showed very high residual stresses in the HAZ and, in addition, a high stress level in the weld metal.

It can be assumed that these high stresses result on the one hand from the comparably rigid weld surroundings in relation to the short weld length and on the other hand from interactions with the transverse residual stresses at the magnitude of the yield point in the weld metal bulk.

The basic experiments at the MVT-testing facility in varestreint mode under different test conditions (cf. Figs. 8 and 9) exhibit—in contrast to welding without additional loading (case II, cf. Fig. 13b)—very high residual stresses dependent on the time the external bending load is applied. It was found that longitudinal loading during the cooling of the sample (case III, cf. Fig. 13c) almost completely suppresses the formation of transformation-related compressive residual stresses in the weld. The result is very high residual stresses at the magnitude of the yield point in the weld seam and rather low residual stress levels in the weld vicinity/HAZ, which represents the case of a short but highly restrained weld, corresponding to the slot specimen set-up (cf. Figs. 6b and 11). Applying a longitudinal bending load during welding led to a moderate residual stress level in the weld seam. But it resulted in residual stress levels at the magnitude of the yield strength in the weld vicinity or HAZ, which typically occurs in welds with high longitudinal shrinkage restraint due to the weld length and thickness, corresponding with the results of the U-shape notch specimen set-up (cf. Figs. 6a and 10).

Thus, it is shown that component relevant longitudinal welding stresses can be applied to small laboratory samples with external bending stress using the MVT-testing facility in varestreint mode even with parameters close to the standard settings by comparison with the residual stresses found in the mock-up test specimens, cf. Table 3. It was even possible to achieve virtual isolation of the cases of highest residual stresses in the weld metal and highest residual stresses in the HAZ and, in addition, the achievable stresses can be increased to a level in the range of the material strength. Similar to these findings, also component-relevant welding-induced stresses transverse to the weld direction should be achievable with the MVT-test set-up in transvarestreint mode. This is emphasised due to the observation that very high transverse restraints lead to maximum residual stresses rather in the weld metal, and, additionally, very high bending restraints cause significantly increased residual stresses in the HAZ or weld vicinity. This should be focus in future investigations.

The analysed stress distributions and magnitudes are in good agreement with the residual stresses found in the mock-up test specimens and therefore the mechanisms of residual stress evolution due to welding under component relevant restraint conditions. From that, it can be stated that a residual stress assessment for component-related welding maybe conducted at small-scale specimens via the MVT-test. However, future investigations

**Table 3** Comparison of the results regarding restraint and welding stress level for different test set-ups

specimen, set-up / result	U-shape notch specimen, Fig. 6a, 10	slot specimen, Fig. 6b, 11	2-MN-testing facility, Fig. 7, 12	MVT-test (Fig. 8, 9)	
				case III, Fig. 13c	case IV, Fig. 13d
<b>restraint</b>				“short weld”	“long weld”
longitudinal	++	+	O	+	++
transversal	–	++	+	–	–
bending	–	O	++	–	–
<b>long. residual stress</b>					
weld metal (WM)	O	+		++	+
HAZ	++	++		+	++
base metal (BM)	–	O		–	–
<i>approx. maximum residual stress</i>	400 MPa, HAZ/ weld vicinity	400 MPa, WM and HAZ		600 MPa (YS), WM	600 MPa (YS), HAZ
<b>trans. residual stress</b>					
weld metal (WM)	O	++	++		
HAZ	O	+	++		
base metal (BM)	–	+	+		
<i>approx. maximum residual stress</i>	100 MPa, WM	600 MPa (YS), WM (bulk)	500 MPa, WM; 300 MPa, HAZ		

**symbols:** (++) very high; (+) high; (O) moderate; (–) no effect/not applicable; (YS) stress at yield point of BM

regarding detailed residual stress assessment and testing of the SRC behaviour of low alloyed creep-resistant steels should consider further improvements and suggestions for the test procedure, see section 5.

## 4 Conclusions

Welding stresses and, therefore, the restraint condition during welding significantly affect the SRC behaviour. Therefore, welding stresses have to be quantified and assessed prior to PWHT. It could be shown that component-specific influences and interactions for SRC testing are necessary, which would result in a systematic SRC testing on actual components or large weld mock-ups. In most cases, this would be too expensive or impossible to realise. Based on the results of experiments and residual stress analysis, this paper discusses approaches and opportunities to systematically investigate and include all three main influencing factors considering their respective complex interactions and interdependencies, in straightforward and easy-to-implement test procedures. The aim was to obtain basic findings about the build-up of residual welding stresses as a function of the type and intensity of the shrinkage and distortion restraint, as it occurs in actual component welds, and to transfer them to small externally loaded laboratory samples. The main conclusions are as follows:

1. A stepwise downscaling from component welds to component-related mock-up and large testing facility

set-up to simple laboratory test set-ups can be achieved, applying the restraint intensity concept, by means of longitudinal, transversal, and bending restraint intensity factors or classification.

2. The analysis of component restraint conditions in different experimental set-ups (U-shape notch specimen, slot specimen, specimen in 2-MN-testing facility) and assessment of welding residual stresses due to typical SAW process conditions for welding of thick-walled creep-resistant steels showed a significant influence of restraint intensity on the residual stress level.
3. It is also shown that surface residual stresses of component welds might underestimate the actual stress condition of the component, which emphasises the importance of the comparative analysis of bulk residual stresses, i.e. using neutron diffraction.
4. Using the analysed residual stress data in context with the corresponding restraint conditions, a transference of component-specific conditions to external loaded specimen in the MVT-testing facility is achievable.
5. First basic experiments were conducted at the MVT-testing facility using GTAW at BM specimens in varestreint mode. Applying bending loads longitudinal to the weld seam during welding and during cooling represents two extreme case studies for very long and very short highly restrained weld seams, respectively. The results were either high tensile stress levels at the magnitude of the yield strength in the HAZ/weld vicinity and in the weld metal, for the latter case.

## 5 Outlook and future research

The experimental results enabled the identification of recommendations and improvements for further investigations on such small laboratory specimens using the MVT-test. Thus, several issues have been identified regarding an appropriate small-scale testing of the SRC behaviour, which should be considered and improved in future research:

1. The tests should provide an external loading transverse to weld direction, as shown in Fig. 8b, to represent significant restraint transverse to the welding direction and bending restraint of actual welded components.
2. Further weld tests should also be conducted with specimens machined from weld metal. This is essential, on the one hand, in order to take into account the special microstructure of the weld metal or filler material and, on the other hand, the high residual stresses in the weld metal, which are due to the significantly increased yield strength of the weld metal in as welded condition.
3. Additional experiments are necessary with test conditions that are between the rather extreme scenarios used in this work. This is achievable by a fine adjustment of bending start time  $t_b$ , bending speed  $v_b$ , and bending stroke  $h_b$  for a defined configuration of restraint situations of actual investigated welding cases or actual component welds.
4. A technical solution has to be found that considers the superposition of the residual stresses by the springback of the sample, by exemplary measurements of the residual stresses of the clamped specimen. Regarding more sophisticated bending parameters (transfer of the restraint conditions to  $t_b$ ,  $v_b$ ,  $h_b$ ) or without the use of the extreme test conditions applied in this work, it is even preferable to avoid springback completely by fixing the loaded specimen for instance on a mounting plate.
5. It needs to be evaluated to what extent the GTAW process used in the MVT-test and the associated heat control are capable to reproduce the microstructure characteristic (HAZ, weld metal) of a submerged arc weld joint.
6. Finally, a definitive assessment of the SRC sensitivity or for the assessment of the influence of welding-related stresses on the SRC formation is only possible if a PWHT is carried out, i.e. if the PWHT subsequent to welding is carried out after the residual stress measurement. For this purpose, the specimens should be fixed analogous to (4) before extraction from the MVT-testing facility so that the bending and welding stresses remain in the specimen. This ensures that not only the microstructure welded under restraint (part II, [7]) but also the welding stress itself (part I, [6]) can show their respective influence on the SRC behaviour. In conclusion, it is important to assess whether the small-scale laboratory specimens are suitable for realistically reflecting the effects

and influences that are to be found in these investigations, even if high welding-related stresses in the small specimens are present.

**Code availability** Not applicable.

**Author contribution** Not applicable.

**Funding** Open Access funding enabled and organized by Projekt DEAL.

**Data Availability** Not applicable.

### Declarations

**Ethical approval** We hereby state that the present work is in compliance with the ethical standards.

**Consent to participate** We hereby consent to participate.

**Consent to publish** We hereby consent to publication.

**Conflict of interest** The authors declare no competing interests.

**Open Access** This article is licensed under a Creative Commons Attribution 4.0 International License, which permits use, sharing, adaptation, distribution and reproduction in any medium or format, as long as you give appropriate credit to the original author(s) and the source, provide a link to the Creative Commons licence, and indicate if changes were made. The images or other third party material in this article are included in the article's Creative Commons licence, unless indicated otherwise in a credit line to the material. If material is not included in the article's Creative Commons licence and your intended use is not permitted by statutory regulation or exceeds the permitted use, you will need to obtain permission directly from the copyright holder. To view a copy of this licence, visit <http://creativecommons.org/licenses/by/4.0/>.

## References

1. Antalfy L (2009) Metallurgical, design & fabrication aspects of modern hydroprocessing reactors. *Weld Res Counc Bull* 524:77–115
2. Park K, Kim S, Chang J, Lee C (2012) Post-weld heat treatment cracking susceptibility of T23 weld metals for fossil fuel applications. *Mater Des* 34:699–706. <https://doi.org/10.1016/j.matdes.2011.05.029>
3. Nevasmaa P, Salonen J (2013) Reheat cracking susceptibility and toughness of 2% CrMoWVNb P23 steel welds. *Weld World* 52(3–4):68–78. <https://doi.org/10.1007/bf03266633>
4. Lausch T (2015) Untersuchungen zum Einfluss der Wärmeleitung auf die Rissbildung beim Spannungsarmglühen dickwandiger Bauteile aus 13CrMoV9-10. Dissertation, BAM Bundesanstalt für Materialforschung und -prüfung, BAM Dissertationsreihe Band 134. Otto-von-Guericke-Universität Magdeburg, Berlin (in German).
5. Lausch T, Kannengiesser T, Schmitz-Niederer M (2013) Multi-axial load analysis of thick-walled component welds made of 13CrMoV9-10. *J Mater Process Technol* 213:1234–1240. <https://doi.org/10.1016/j.jmatprotec.2013.01.008>

6. Kromm A, Lausch T, Schroepfer D, Rhode M, Kannengiesser T (2020) Influence of welding stresses on relief cracking during heat treatment of a creep-resistant 13CrMoV steel: part I—effect of heat control on welding stresses and stress relief cracking. *Weld World* 64(5):807–817. <https://doi.org/10.1007/s40194-020-00875-6>
7. Kromm A, Lausch T, Schroepfer D, Rhode M, Kannengiesser T (2020) Influence of welding stresses on relief cracking during heat treatment of a creep-resistant 13CrMoV steel part II: mechanisms of stress relief cracking during post weld heat treatment. *Weld World* 64(5):819–829. <https://doi.org/10.1007/s40194-020-00881-8>
8. Rhode M, Kromm A, Schroepfer D, Steger J, Kannengiesser T (2018) Residual stress formation in component related stress relief cracking tests of a welded creep-resistant steel. In: *Proceedings, Residual Stresses 2018: ECRS-10. Materials Research Forum*, pp 185–190. <https://doi.org/10.21741/9781945291890-29>
9. Kromm A, Lausch T, Schröpfer D, Dixneit J, Hannemann A, Kannengiesser T (2018) From the field to the lab: real scale assessment of stresses in welded components. *Mater Perform Charact* 7(4):574–593. <https://doi.org/10.1520/MPC20170103>
10. Kannengiesser T, Boellinghaus T (2014) Hot cracking tests—an overview of present technologies and applications. *Weld World* 58(3):397–421. <https://doi.org/10.1007/s40194-014-0126-y>
11. Thomas M, Vollert F, Weidemann J, Gibmeier J, Kromm A, Kannengiesser T (2020) Surface- and volume-based investigation on influences of different Vrestraint testing parameters and chemical compositions on solidification cracking in LTT filler metals. *Weld World* 64:913–923. <https://doi.org/10.1007/s40194-020-00895-2>
12. Kannengiesser T, Boellinghaus T (2013) Cold cracking tests - an overview of present technologies and applications. *Weld World* 57: 3–37. <https://doi.org/10.1007/s40194-012-0001-7>
13. Schroepfer D, Kromm A, Kannengiesser T (2018) Load analyses of welded high-strength steel structures using image correlation and diffraction techniques. *Weld World* 62(3):459–469. <https://doi.org/10.1007/s40194-018-0566-x>
14. Schwenk C, Kannengiesser T, Rethmeier M (2009) Restraint conditions and welding residual stresses in self-restrained cold cracking tests. *Trends in Welding Research: Proceedings of the 8th International Conference, June, 2008, Callaway Gardens Resort, Pine Mountain, Georgia, USA. ASM International*. <https://doi.org/10.1361/cp2008twr766>
15. Sun J, Hensel J, Nitschke-Pagel T, Dilger K (2019) Influence of restraint conditions on welding residual stresses in H-type cracking test specimens. *Materials (Basel)* 12(17). <https://doi.org/10.3390/ma12172700>
16. Schroepfer D, Kromm A, Kannengiesser T (2018) Formation of multi-axial welding stresses due to material behaviour during fabrication of high-strength steel components. *Weld World* 63(1):43–51. <https://doi.org/10.1007/s40194-018-0650-2>
17. Schroepfer D, Kromm A, Hannemann A, Kannengiesser T (2018) In-situ determination of critical welding stresses during assembly of thick-walled components made of high-strength steel. In: *Proceedings, Residual Stresses 2018: ECRS-10. Materials Research Forum*, pp 191–196. <https://doi.org/10.21741/9781945291890-30>
18. Satoh K, Ueda Y, Matsui S, Natsume M, Terasaki T, Fukuda K, Tsuji M (1977) Japanese studies on structural restraint severity in relation to weld cracking. *Weld World* 15:155–189
19. Satoh K, Nakajima H, Toyosada M (1972) Restraint intensity of weld joints in the structural members consisting of plates and stiffeners, IIW-Doc X-660-72
20. Masubuchi K (1980) Analysis of welded structures: residual stresses, distortion, and their consequences.
21. DeGarmo E, Meriam J, Johanssen F (1946) The effect of weld length upon the residual stresses of unstrained butt welds. *Weld J* 25:485–486
22. Altenkirch J, Steuwer A, Peel M, Richards DG, Withers PJ (2008) The effect of tensioning and sectioning on residual stresses in aluminium AA7749 friction stir welds. *Mat Sci Eng A* 488(1-2):16–24. <https://doi.org/10.1016/j.msea.2007.10.055>
23. Dixneit J, Kromm A, Boin M, Wimpory RC, Kannengiesser T, Gibmeier J, Schroepfer D (2017) Residual stresses of LTT welds in large-scale components. *Weld World* 61(6):1089–1097. <https://doi.org/10.1007/s40194-017-0502-5>
24. Withers PJ, Bhadeshia HKDH (2001) Overview - residual stress part 1 - measurement techniques. *Mater Sci Tech Ser* 17(4):355–365. <https://doi.org/10.1179/026708301101509980>
25. Withers PJ, Bhadeshia HKDH (2001) Overview - residual stress part 2 - nature and origins. *Mater Sci Tech Ser* 17(4):366–375. <https://doi.org/10.1179/026708301101510087>
26. Nitschke-Pagel T, Wohlfahrt H (2002) Residual stresses in welded joints - sources and consequences. *Mater Sci Forum* 404–407:215–226. <https://doi.org/10.4028/www.scientific.net/MSF.404-407.215>
27. Wohlfahrt H (1987) Residual stresses as a consequence of welding. *Advances in Surface Treatments Vol. 4 - International Guidebook on Residual Stresses*.
28. Dai H, Francis JA, Stone HJ, Bhadeshia HKDH, Withers PJ (2008) Characterizing phase transformations and their effects on ferritic weld residual stresses with X-rays and neutrons. *Metall Mater Trans A* 39: 3070–3078. <https://doi.org/10.1007/s11661-008-9616-0>
29. Schroepfer D, Kromm A, Schaupp T, Kannengiesser T (2018) Welding stress control in high-strength steel components using adapted heat control concepts. *Weld World* 63(3):647–661. <https://doi.org/10.1007/s40194-018-00691-zb>

**Publisher's note** Springer Nature remains neutral with regard to jurisdictional claims in published maps and institutional affiliations.